Transactions of the Materials Research Society of Japan 30[1] 303-306 (2005)

Formation of amorphous-CN thin films by the deposition of CN radicals—Absolute density of gas-phase CN

Haruhiko Ito, Hidetoshi Saitoh
Department of Chemistry, Nagaoka University of Technology, Nagaoka 940-2188, Japan
Fax: 81-258-47-9300, e-mail: bu7dd8@nagaokaut.ac.jp

The absolute density of the CN($X^2\Sigma^+$) radicals produced by the dissociative excitation reaction of BrCN with the microwave (MW) discharge flow of Ar was measured by use of the laser-induced fluorescence (LIF) spectroscopy of the CN($A^2\Pi_i$-$X^2\Sigma^+$), 4-0, 5-1, and 7-2 bands. The pressure of Ar was 0.1 Torr. The LIF intensity for the individual transition was evaluated by the spectral simulation analysis and by the calibration against Rayleigh scattering intensity. The absolute density of CN($X^2\Sigma^+$) was evaluated as 1.6×10^{19} m^{-3} which was much larger than the previously determined densities of Ar($^3P_2$) and Ar^+, 4.05×10^{14} and 8.46×10^{15} m^{-3}, respectively. According to a kinetic analysis, the production and loss processes of the CN($X^2\Sigma^+$) radicals are, predominantly, the charge transfer from Ar^+ followed by the $BrCN^+$-e^- recombination and the reaction with BrCN, respectively.

Key words: CN radicals, LIF, number density, microwave plasma, amorphous carbon nitride

1. INTRODUCTION

Amorphous carbon nitrides (a-CN_x) and hydrogenated amorphous carbon nitrides (a-CN_x:H) have attracted much attention due to their important properties such as high hardness [1], field emission [2], capacity for hydrogen storage [3]. One of the central problems of the processing of a-CN_x has been the development of the methodology incorporating the nitrogen atoms effectively [1]. We have applied the dissociative excitation reactions of BrCN and CH_3CN with the microwave (MW) discharge flow of Ar to the CVD processes to form a-CN_x or a-CN_x:H [4,5]. These reactions produce CN radicals with high efficiency [6,7]. According to our systematic studies on the film properties and on the spectroscopic observations, the following characteristics have been found when BrCN is used as the starting material.

(A) The [N]/([N]+[C]) ratio of the film is as high as 50% [4]. Under the condition that the water molecules are removed from the reaction system *and* the RF-bias voltage is applied to the substrate, the hardness of the films can reach as high as that of the diamond-like carbon (DLC) films [5]. (B) The CN($B^2\Sigma^+$–$X^2\Sigma^+$) emission spectra have been observed under the same experimental conditions as the film formation, and it is indicated that the CN($B^2\Sigma^Y$) state is formed *via* the energy transfer from the metastable atoms of Ar, Ar($^3P_{0,2}$),

$$Ar(^3P_{0,2}) + BrCN \rightarrow CN(B^2\Sigma^+) + Br + Ar, \quad (1)$$

and the charge transfer from Ar^+ followed by the recombination with free electrons [8],

$$Ar^+ + BrCN \rightarrow BrCN^+ + Ar \quad (2)$$

$$BrCN^+ + e^- \rightarrow CN(B^2\Sigma^+) + Br. \quad (3)$$

The excitation energies of (A) and (B) are 11.5-11.8 eV, being smaller than that of the formation of carbon atoms, 12 eV. Therefore, it is strongly suggested that the precursors of the film formation are, predominantly, the ground-state CN radicals.

According to the above discussion, it is effective to analyze the formation process of CN($X^2\Sigma^+$) radicals. Based on this motivation, the present study reports on the density measurement of CN($X^2\Sigma^+$) produced by the decomposition of BrCN in the MW discharge flow of Ar. Analogous to our previous publication, the CN($X^2\Sigma^+$) radicals are monitored by observing the laser-induced fluorescence (LIF) spectrum of the CN($A^2\Pi_i$–$X^2\Sigma^+$) transition whose intensity, I_{LIF}, is calibrated against Rayleigh scattering intensity, I_R [9]. The density of CN($X^2\Sigma^+$) is compared with the densities of Ar($^3P_2$) and Ar^+ which have been determined by using, respectively, the LIF spectroscopy and electrostatic-probe method in our previous study [10]. Then, the processes of formation and loss of CN($X^2\Sigma^+$) are discussed.

2. EXPERIMENTAL

Figure 1 shows schematically the MW chemical vapor deposition (MWCVD) apparatus used in the present study. The apparatus was essentially the same as that used in our previous studies [6-8]. The reaction chamber with an inner diameter of 4 inches was evacuated to 10^{-3}

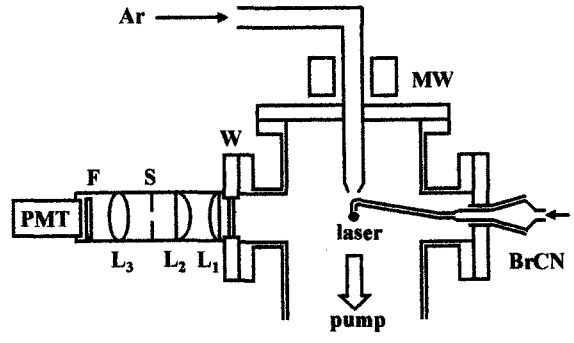

Fig. 1 MWCVD apparatus used in the present study

Torr using a combination of mechanical-booster (110 m^3/h) and oil-rotary (670 L/min) pumps. A discharge tube with an outer diameter of 15 mm made of Pyrex glass was set at the upper part of the reaction chamber. The tip of the discharge tube was reduced to ≈3 mm and was positioned ≈10 mm above the laser-beam path. Ar gas was introduced into the discharge tube through a stainless-steel needle valve without purification. The pressure of Ar, P_{Ar}, was 0.1 Torr. The Ar plasma flow was produced by MW discharge (2.45 GHz, 100 W). BrCN was introduced into the reaction chamber through a Teflon needle valve and a stainless-steel nozzle with an inner diameter of 1 mm whose tip was placed ≈5 mm downstream of that of the discharge tube. CN radicals formed just downstream of the nozzle tip were excited by a dye-laser beam from the $X^2\Sigma^+$ state to the $A^2\Pi_i$ state. The $A^2\Pi_i$–$X^2\Sigma^+$ LIF signal generated at a right angle to the dye-laser beam was monitored through three lenses (L_1, L_2, and L_3), a slit (S), and a photomultiplier tube (PMT) (Hamamatsu R955). The width and height of S were set to be 10 and 1 mm, respectively; the image of S at the center of the chamber was made to coincide with the laser beam whose cross section was nearly circular with the diameter of ≈3 mm. Then, the fluorescence generated in the volume of ≈30 mm^3 was collected. A sharp-cut filter (F) was set in front of PMT in order to cut the wavelength shorter than 520 nm. In order to prevent the undesired scattering laser radiation, the inner wall of the chamber was coated with Aquadag (Acheson). By use of the above experimental setup, the effects of the undesired background emission and stray light are effectively excluded.

Figure 2 shows a schematic diagram of the system for observing the LIF spectrum and the effective lifetime. A pulsed dye laser (Quantel TDL-60) excited by the second harmonic of a Nd:YAG laser (Quantel YG-661-20) was used to observe the CN($A^2\Pi_i$–$X^2\Sigma^+$) LIF spectrum. The wavelength of the dye laser was 618–627 nm for the observation of the CN($A^2\Pi_i$–$X^2\Sigma^+$), 4–0 band, 632-641 nm for the 5-1 band, and 585-592 nm for the 7-2 band. The power of the dye-laser beam was typically 2 mJ/pulse, where the saturation condition was fulfilled. In the observation of the LIF spectrum, the pulsed LIF signal from PMT was terminated by a 50 kΩ resistor to obtain a sufficient voltage signal, and processed by two boxcar integrators (Stanford SR250), labeled A and B in Fig. 2. The sampling-gate widths of A and B were set at 15 μs, and the delay of the sampling gate of B to that of

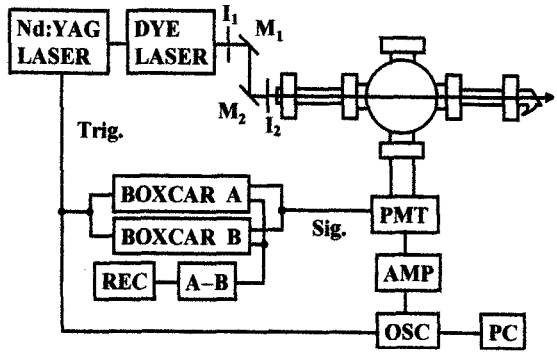

Fig. 2 Experimental setup for observing LIF spectra

A was set to be 60 μs where the LIF signal was not detected. Other conditions such as sensitivity and integration time were set to be equal for A and B. Then, the difference A–B was recorded by a chart recorder (REC). By means of the above process, the background signal could be completely eliminated. In the observation of the effective lifetime, the LIF signal from PMT was terminated by a 50 Ω resistor, and processed by a fast preamplifier (Stanford SR445, denoted as AMP), and monitored by a digital storage oscilloscope (LeCroy LT372, denoted as OSC) and a personal computer (PC).

The intensity of Rayleigh scattering from Ar, I_R, was measured using the same apparatus as above, where P_{Ar} was varied in the range of 0–7 Torr. The power of the dye-laser beam was the same as that in the LIF measurement (2 mJ/pulse). The intensity of the scattering signal at P_{Ar}=6 Torr was observed to be comparable with the LIF intensity. Scattering signal from the wall of the apparatus was negligible. Then, I_R at P_{Ar}=6 Torr was used for the calibration of the LIF intensity.

3. RESULTS AND DISCUSSION

3.1 Number density of CN($X^2\Sigma^+$)

Figs. 3(a), 4(a), and 5(a) show the observed LIF spectra of the CN($A^2\Pi_i$–$X^2\Sigma^+$), 4-0, 5-1, and 7-2 bands, respectively, with the assignments of the spectral lines [11]. As shown in these figures, almost all the spectral lines overlap. In order to evaluate the relative intensity of the individual LIF transition, the observed spectra were simulated by adjusting the relative intensity, $I_{v''\Omega''J''}^{v'\Omega'J'}$, where J denotes the quantum number of the total angular momentum and Ω its projection on the internuclear axis. Figs. 3(b), 4(b), and 5(b) show the simulated spectra of the 4-0, 5-1, and 7-2 bands, respectively. It is confirmed that the observed spectra are fully reproduced by the simulated spectra. Figs. 6, 7, and 8 show the intensity distributions of the rotational branches. The relative intensities of the transitions belonging to the individual branch are confirmed to make a smooth distribution. The radiative decay was observed by monitoring the R_2 band head of the 4-0 band to yield the effective lifetime, τ_{eff}, to be 1.1 μs.

Based on the above results, the number density of the (v'', Ω'', J'')-th level of the CN($X^2\Sigma^+$) radicals, $n_{v''\Omega''J''}$, corresponding to the individual transition was evaluated

$$n_{v''\Omega''J''} = \frac{I_{v''\Omega''J''}^{v'\Omega'J'}}{I_R}\frac{g_2}{g_1}\frac{E_R}{h\nu_{v''\Omega''J''}^{v'\Omega'J'}}\frac{4\pi}{S_L}\frac{d\sigma_{Ar}}{d\omega}\frac{n_{Ar}}{\tau_{eff}} \times\left(\sum_{v\Omega J}A_{v'v}\frac{S_{\Omega J}^{\Omega'J'}}{2J'+1}S_e(\lambda_{v'v})\right)^{-1} Se(\lambda_R). \quad (4)$$

The symbols appearing in eq. (4) are as follows. The degeneracies of the initial and final levels of the laser absorption are represented as g_1 and g_2, respectively. E_R and $\nu_{v''\Omega''J''}^{v'\Omega'J'}$ are the laser energy and the transition wavenumber, respectively. S_L is the cross-sectional area of the dye-laser beam, and $d\sigma_{Ar}/d\omega$ is the differential cross section of Rayleigh scattering per unit solid angle, ω [12]. $A_{v'v}$ and $S_{\Omega J}^{\Omega'J'}$ are the Einstein coefficient [13] of the v'–v fluorescence transition and the Hönl-London factor [14], respectively. $S_e(\lambda_{v'v})$ and $S_e(\lambda_R)$ are the

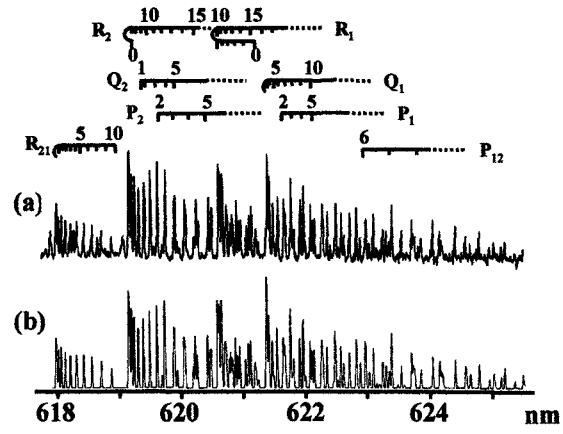

Fig. 3 LIF spectra of the CN($A^2\Pi_i$–$X^2\Sigma^+$) 4-0 band (a) observed (b) simulated

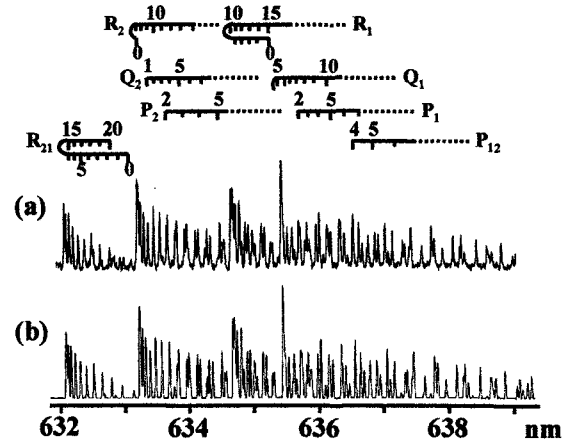

Fig. 4 LIF spectra of the CN($A^2\Pi_i$–$X^2\Sigma^+$) 5-1 band (a) observed (b) simulated

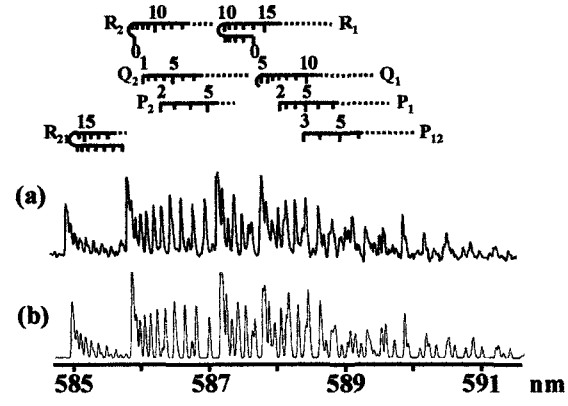

Fig. 5 LIF spectra of the CN($A^2\Pi_i$–$X^2\Sigma^+$) 7-2 band (a) observed (b) simulated

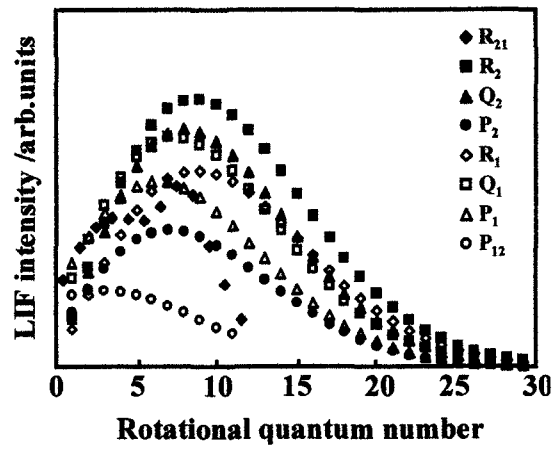

Fig. 6 LIF intensity distribution determined in the spectral simulation of the CN($A^2\Pi_i$–$X^2\Sigma^+$), 4-0 band

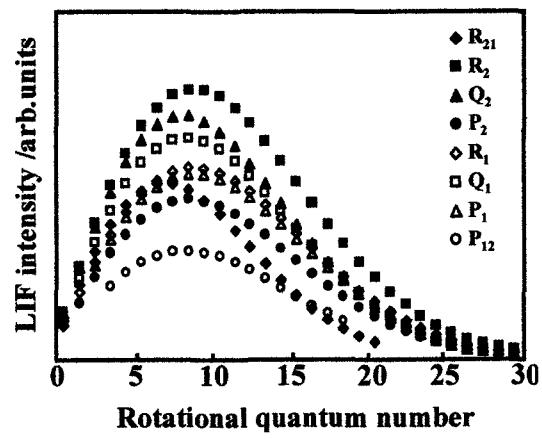

Fig. 7 LIF intensity distribution determined in the spectral simulation of the CN($A^2\Pi_i$–$X^2\Sigma^+$), 5-1 band

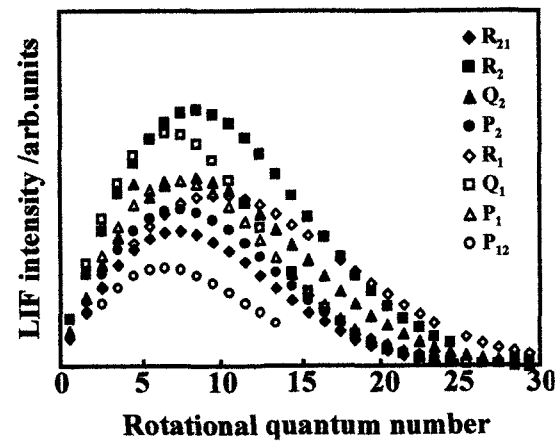

Fig. 8 LIF intensity distribution determined in the spectral simulation of the CN($A^2\Pi_i$–$X^2\Sigma^+$), 7-2 band

sensitivities of the detection system for the fluorescence transition and Rayleigh scattering, respectively.

The number densities of the CN($X^2\Sigma^+$), v"=0-2 levels, $n_{v"}$, were evaluated as

$$n_{v"} = \sum_{\Omega"J"} n_{v"\Omega"J"}, \quad (5)$$

They are listed in Table I. It was confirmed that the densities of the v"≥3 levels were negligible. Then, the total number density of CN($X^2\Sigma^+$) is evaluated by summing up the densities listed in Table I as

$$n=1.6\times10^{19}\ m^{-3}. \quad (6)$$

This value is 4-5 orders of magnitude larger than the previously determined densities of Ar($^3P_2$) and Ar^+, 4.05×10^{14} and 8.46×10^{15} m^{-3}, respectively, in the neat Ar plasma flow [10].

v	$n_{CN(X),v}/m^{-3}$
0	1.1×10^{19}
1	4.4×10^{18}
2	6.9×10^{17}

Table I Density (n) of the CN($X^2\Sigma^+$) radicals in the gas phase (in m^3 units)

3.2 Kinetic analysis of CN($X^2\Sigma^+$)

As described in ref. [10], the Ar^+ density is 2.0×10^{15} m^{-3} when BrCN is introduced into the reaction system. On the other hand, the Ar($^3P_{0,2}$) density becomes negligibly small. Therefore, the dominant process of decomposition of BrCN is process (B) described in section 1. The discussion given below indicates that reaction (2) is rate-determining. The electrons having kinetic energy lower than the ionization energy of BrCN (11.9 eV) [15] contribute to the $BrCN^+$-e^- recombination (reaction (3)). The proportion of the electrons contributing to this reaction is evaluated by a numerical integration of the electron-energy distribution reported in ref. [10] as ≈99%. Thus, almost all the electrons can contribute to the $BrCN^+$-e^- recombination. According to the recombination constants for CO_2^+ and N_2O^+ ($k_{rec}\approx10^{-13}$ m^3s^{-1}) [16] and the rate constants for the charge transfer from Ar^+ to CH_4 and NH_3 ($k_{ct}\approx10^{-16}$ m^3s^{-1}) [17], the k_{rec} values are ≈3 orders of magnitude higher than k_{ct}. Hence, the rate constant of reaction (3) is expected to be much larger than that of reaction (2).

The main loss process of CN($X^2\Sigma^+$) is considered to be the reaction with BrCN [18]

$$CN(X^2\Sigma^+) + BrCN \rightarrow Br + C_2N_2,$$
$$k_Q=2.1\times10^{-19}\ m^3s^{-1}. \quad (7)$$

According to the formation and loss processes of CN discussed above, the concentration of CN radicals can be evaluated as

$$[CN]\approx[Ar^+]k_{ct}/k_Q \quad (8)$$

$[Ar^+]$ has been evaluated in our previous report to be 8.46×10^{15} m^{-3}. Therefore, [CN] in eq. (8) is evaluated as 1×10^{18} m^3. This value is one order of magnitude smaller than the observed value, 1.6×10^{19} m^{-3}. The discrepancy between the observed and calculated values can be attributed to the uncertainty of the k_{ct} value. The above discussion suggests that the dominant processes of formation and loss of CN radicals are eqs. (2)-(3) and (7), respectively.

4. CONCLUSION

The present study reports on the LIF spectroscopic measurement of the CN($X^2\Sigma^+$) radicals which are formed from the dissociative excitation reaction of BrCN with the MW discharge flow of Ar. The density of CN($X^2\Sigma^+$) is found to be ≈4-5 orders of magnitude larger than the densities of Ar($^3P_2$) and Ar^+ reported in our previous study [10]. A simple kinetic analysis indicates that the production and loss processes of the CN($X^2\Sigma^+$) radicals are, predominantly, the charge transfer from Ar^+ followed by the $BrCN^+$-e^- recombination and the reaction with BrCN, respectively.

ACKNOWLEDGEMENTS

The authors thank to Mr. Yoshinori Sato for his technical assistance. This work was supported by Grants-in-Aid for Scientific Research, from the Ministry of Education, Culture, Sports, Science, and Technology, under Contract Nos. 13555197, 14550721, and 16040208.

References

[1] W. Kulisch, "Deposition of Diamond-Like Superhard Materials", Springer-Verlag, Berlin, (1999) pp. 112-20.
[2] Y. Ohkawara, T. Naijo. T. Washio, S. Ohshio, H. Ito and H. Saitoh, Jpn. J. Appl. Phys., **40**, 7013-17, (2001).
[3] Y. Ohkawara, S. Ohshio, T. Suzuki, K. Yatsui, H. Ito and H. Saitoh, Jpn. J. Appl. Phys., **40**, 3359-63, (2001).
[4] H. Saitoh, H. Takamatsu, D. Tanaka, N. Ito, S. Ohshio and H. Ito, Jpn. J. Appl. Phys., **39**, 1258-63, (2000).
[5] D. Tanaka, Y. Ohkawara, N. Ito, S. Ohshio, H. Ito and H. Saitoh, Jpn. J. Appl. Phys., **39**, 4148-52, (2000).
[6] H. Ito, N. Ito, T. Takahashi, H. Takamatsu, D. Tanaka and H. Saitoh, Jpn. J. Appl. Phys., **39**, 1371-77, (2000).
[7] H. Ito, N. Ito, T. Takahashi, D. Tanaka, H. Takamatsu and H. Saitoh, Jpn. J. Appl. Phys., **40**, 332-37, (2001).
[8] H. Ito, K. Tanaka, A. Sato, N. Ito, Y. Ohkawara and H. Saitoh, Jpn. J. Appl. Phys., **41**, 3130-36, (2002).
[9] H. Ito, S. Ichimura, K. C. Namiki and H. Saitoh, Jpn. J. Appl. Phys. **42**, 7116-21, (2003).
[10] H. Ito, Y. Sato, and H. Saitoh, Jpn. J. Appl. Phys. **43**, 7277-7281, (2004).
[11] S. P. Davis and J. G. Phillips, "The Red System ($A^2\Pi$-$X^2\Sigma$) of the CN Molecule", University of California Press, Berkeley, (1963) pp.89-94.
[12] A. W. DeSilva and G. C. Goldenbaum, "Methods of Experimental Physics", vol. 9, ed. by H. R. Griem and R. H. Lovberg, Academic Press, New York, (1970) pp. 61-113.
[13] C. W. Bauschlicher Jr., S. R. Langhoff and P. R. Taylor, Astrophys. J., **332**, 531-38, (1988).
[14] I. Kovács, "Rotational Structure in the Spectra of Diatomic Molecules", Adam Hilger, London, (1969) pp. 130-31.
[15] G.W. King and A.W. Richardson: J. Mol. Spectrosc. **21**, 339-352, (1966).
[16] T. Gougousi, M.F. Golde and R. Johnsen: Chem. Phys. Lett. **265**, 399-403, (1997).
[17] D.L. Albritton: At. Nucl. Data Tables **22**, 1-89, (1978).
[18] S. Zabarnick and M. C. Lin, Chem. Phys. **134**, 185-191, (1989).

(Received December 23, 2004; Accepted January 31, 2005)